PERGAMON

International Journal of Heat and Mass Transfer 44 (2001) 1309–1322

International Journal of HEAT and MASS TRANSFER

www.elsevier.com/locate/ijhmt

Determination of heat sources and heat transfer coefficient for two-dimensional heat flow – numerical and experimental study

Refahi Abou khachfe *, Yvon Jarny

Laboratoire de Thermocinetique, Ecole polytechnique de l'universite de Nantes, UMR CNRS 6607, BP 50609, 44306 Nantes, France

Received 20 December 1999; received in revised form 15 May 2000

Abstract

An experimental apparatus and a numerical method are presented to study the determination of both the location and the time-varying strength of point heat sources within a body from temperature boundary measurements. It is shown that the computed solutions of the inverse heat source problems (IHSPs) are correlated to the heat transfer coefficient on the boundary where the temperature sensors are located. The same algorithm is used to determine this coefficient as a function of temperature. It consists in solving a non-linear inverse heat conduction problem for two-dimensional heat flow. The computed solutions of the inverse problems obtained from the temperature histories measured by four thermocouples are compared to the experimental data. The case of two-point sources is also considered.

Keywords: Heat source; Heat transfer coefficient; Optimization; Conjugate gradient method; Iterative regularization

1. Introduction

Numerical methods and computational algorithms for solving two-dimensional inverse heat conduction problems (IHCP) have been extensively developed over the last decade. Based on finite or boundary elements' techniques, they provide an efficient way to analyze transient heat flow within arbitrarily shaped domains. Most of them are devoted to the determination of transient and/or spatially distributed heat flux on the boundary of the body [1–3]. Important applications of these methods have been studied in various branches of thermal engineering area: quenching [4], casting and phase-change process [5–7], hot rolling and welding [8,9]. Few of these works consider experimental situations involving unknown heat sources. Silva Neto and Ozisik [10] used the conjugate gradient algorithm (CGA) to estimate the time-varying strength of a line source placed in a rectangular region with insulated boundaries, but the location of the source was specified. Le Niliot [11] studied linear inverse problems with two-point heat sources, and experimental results were presented in [12]. Yang [13] solved the linear bi-source problem but 1-D heat flow and all these works considered the source locations to be known. Ohmichi and Noda [14] developed a method for the determination of rectangular heat sources for two-dimensional steady state problems. More recently, by using finite elements and the well-known conjugate gradient method, the authors solved two kinds of inverse heat source problems (IHSPs): one deals with the distributed heat source coupled to a chemical reaction which occurs during the cure of thick piece of thermoset polymer [15], and the other is related to point sources and the simultaneous determination of the location and the time-varying strength [16].

In this paper, this method is applied to the inverse analysis of temperature histories measured by thermocouples at the boundary of a slab heated by internal line sources. An experimental set-up has been carefully designed for the study, in order to demonstrate both the efficiency and the limits of the method. It is shown how the heat transfer coefficient at the boundary of the body

* Corresponding author. Tel.: +33-240-683140; fax: +33-240-683141.

E-mail addresses: refahi@isitem.univ-nantes.fr (R. Abou khachfe), jarny@isitem.univ-nantes.fr (Y. Jarny).

0017-9310/01/$ - see front matter
PII: S0017-9310(00)00186-1

Nomenclature

$C(T)$	heat capacity
F_i	spatial distribution of the heat source S_i
$h(T)$	heat transfer coefficient
J	temperature residual criterion
J'	gradient of the functional J
L	Lagrangian
n_{opt}	regularization parameter
P	strength of the line source
Ns	number of thermocouples
Nt	number of time step
S_i	heat source
T	temperature
$\underline{U}$	unkown vector
x_i, y_i	location of the heating wire

Greek symbols

Γ_i	boundary surface
λ	thermal conductivity
ρ	density
σ	standard deviation of temperature residuals
ψ	adjoint function
δT	sensitivity function
Ω	spatial domain

must be accurately determined as a function of temperature, before solving the IHSP when experimental data are used as additional information.

The paper includes six sections. In Section 2, the experimental apparatus is presented together with the modeling equations of the direct heat conduction problem. In Section 3, the main features of the numerical algorithm used for solving both the inverse boundary coefficient problem (IBCP) and the IHSP are recalled. Results of numerical experiments are presented in Section 4. Experimental results concerning the simultaneous determination of the location and the strength of the heat sources are analyzed in Section 5. Finally, the overall contribution and possible applications of this work to the field of inverse heat conduction problems are concluded in the last section.

2. Experimental apparatus – modeling equations

The apparatus in Fig. 1 consists of a plexiglas slab with a rectangular cross-section $L = 50.32$ mm, $\ell = 24.80$ mm; the height of the parallelepiped is $H = 150$ mm. Transient heat transfers are considered within the rectangular domain: $|x| < L/2, 0 < y < \ell$, located in the Oxy plane, at the middle of the slab ($z = H/2$). The z-direction is vertical and the slab is put inside a box, the wall of which is black painted and its temperature is controlled to be a constant equal to T_e. Heat flow at the boundary of the slab results of convective and radiative heat transfers. Four electrical wire heaters (diameter $\phi = 0.5$ mm) are installed within the slab, parallel to the z-axis. In the Oxy plane, the heat sources $S_i, i = 1, \ldots, 4$ are circular, they are assumed to be point sources, their locations (x_i, y_j) are shown in Fig. 1(b). The location errors of the point sources are less than 25×10^{-5} m, that is the value of the wire radius. Temperature is measured at six points with chromel–alumel thermocouples (diameter $\phi = 0.080$ mm). They are installed parallel to the z-direction, four of them on the boundary, and the two others in the middle of the slab. The six welding points are located in the same Oxy plane as shown in Fig. 1(a). Installation of the heaters and thermocouples inside the body was achieved by cutting the slab into six parts, the cutting planes (parallel to Oyz) being located at the same abscissa with the heaters and the internal thermocouples: $x = \pm 18.86$, ± 5.32 mm and $x = 0$. Then, the six parts are stuck together including the wires, each wire has been carefully put in a good-sized groove. The electrical resistance of the heating wires is $R = 50\ \Omega$/m. Two distinct electrical circuits as shown in Fig. 1(c) are used to supply the line sources. Each of them includes two identical line sources (I_1), (I_2) in order to have a symmetrical configuration with respect to the Oyz plane during heating. The strength of the line sources (I_i) (per unit of length) is

$$P_i = \frac{U_i V_i}{2Hr}\ (\mathrm{W/m}), \quad i = 1, 2. \tag{1}$$

The voltage histories $U_i(t)$ and the resulting currents $V_i(t)/r$ in the line source (I_i) are recorded during the experiment to determine the strength $P_i(t)$ according to Eq. (1). These experimental values are compared in Section 5 to the computed solutions of the IHSPs. The thermal properties of plexiglas have been carefully determined [17] in the temperature range (20°C, 120°C), the thermal conductivity is constant $\lambda = 0.19 \pm 0.01$ W/m K, the density is $\rho = 1182$ kg/m^3, and the heat capacity is slowly varying with temperature

$$20 < T \leqslant 100°\mathrm{C}, \quad C_p(T) = 6.77125T + 1160.44,$$
$$100 \leqslant T \leqslant 120°\mathrm{C}, \quad C_p(T) = 18.31T - 1.98.$$

Due to the symmetrical configuration, heat transfers are studied in the rectangular domain $\Omega = \{(x, y), 0 < x < L/2, 0 < y < \ell\}$. The boundary $\Gamma = \Gamma_1 \cup \Gamma_2$ of the domain is defined as in Fig. 2.

The boundary Γ_2 is adiabatic. Heat flux on the boundary Γ_1 is modeled by a Fourier condition with a

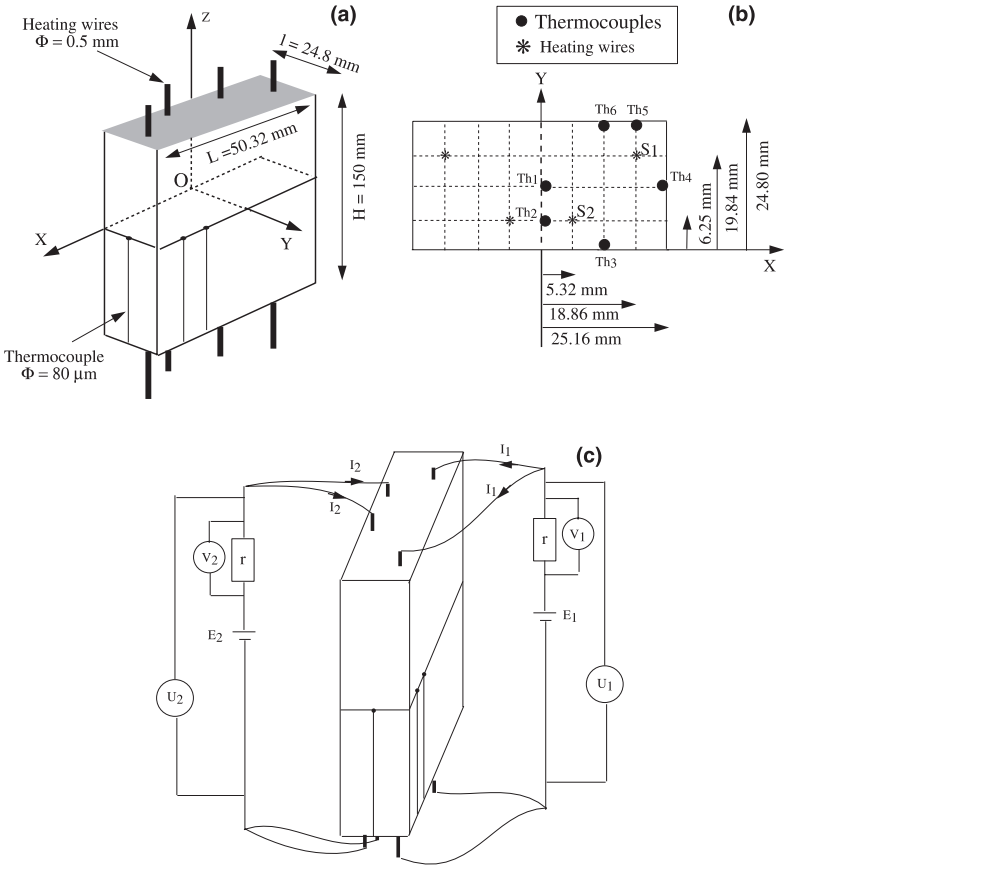

Fig. 1. Experimental apparatus: (a) plexiglas slab; (b) location of the thermocouples and heating wires in the *Oxy* plane; (c) electrical circuits of heating wires.

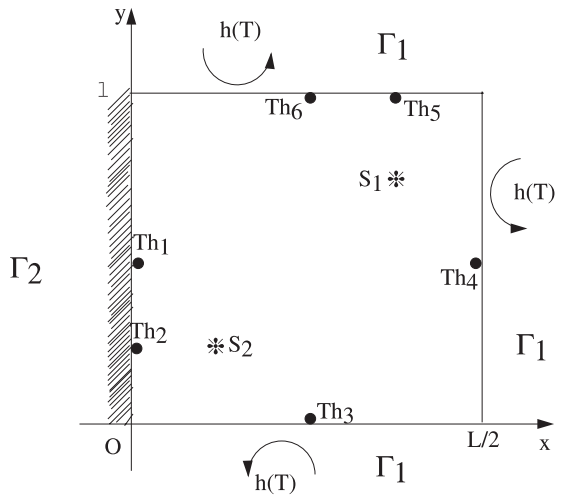

Fig. 2. Spatial domain Ω.

global temperature-varying heat transfer coefficient $h(T)$ which is the sum of a convective coefficient $h_C(T)$ and a radiative coefficient $h_r(T)$. The radiative part of the boundary heat flux is linearized in the temperature range of the experiment.

The transient temperature $T(x,y,t)$ in the rectangular domain Ω is the solution of the following heat conduction equations:

$$\rho C_p(T)\frac{\partial T}{\partial t} - \lambda \Delta T = S, \quad t > 0 \text{ in } \Omega, \tag{2a}$$

$$\lambda \frac{\partial T}{\partial n_1} + h(T)T = h(T)T_e, \quad t > 0 \text{ on } \Gamma_1, \tag{2b}$$

$$\lambda \frac{\partial T}{\partial n_2} = 0, \quad t > 0 \text{ on } \Gamma_2, \tag{2c}$$

$$T = T_0 \quad t = 0 \text{ in } \Omega, \tag{2d}$$

where the initial condition T_0 is supposed to be uniform in Ω. The heat source $S(x,y,t)$ is time-varying, spatially distributed and modeled by the equations

$$S(x,y,t) = \sum_{i=1}^{2} P_i(t)F_i(x,y), \tag{3}$$

$$F_i(x,y) = \frac{1}{\pi\omega^2}\exp\left(-\frac{(x-x_i)^2+(y-y_i)^2}{\omega^2}\right), \quad i=1,2. \tag{4}$$

It is assumed that the location (x_i, y_i) is far enough from the boundary Γ to have

$$\int_\Omega F_i \,\mathrm{d}\Omega = 1, \quad i=1,2 \quad \text{then} \quad \int_\Omega S(x,y,t)\,\mathrm{d}\Omega = P_1(t)+P_2(t). \tag{5}$$

Modeling the point source by Eqs. (3) and (4) is correct if the value of the scalar ω is taken as less than or equal to the radius of the heating wires ($\phi = 0.5$ mm). In practice, it is sufficient to take ω equal to the mesh size of the finite element grid. The numerical solution of Eqs. (2a)–(2d) is computed by using a standard finite element technique which is well adapted to solve this transient two-dimensional non-linear heat conduction problem. For computational convenience, the parameter functions $\rho C_p(T)$, $h(T)$ are approximated in the form

$$f(T) = \sum_{i=1}^{Np} f_i\varphi_i(T) \text{ with } f_i = f(T_{\mathrm{tab},i}),$$

where $[\varphi_i]_{i=1}^{Np}$ is a given set of Np basis functions over the temperature interval under study. This interval is divided into $Np-1$ subintervals $[T_{\mathrm{tab},i-1}, T_{\mathrm{tab},i}]$ and $[T_{\mathrm{tab},i}]_{i=1}^{Np}$ is a priori given. Piecewise linear functions or natural spline functions are usually used in practice. Numerical simulations of the heating experiments are presented in Section 4. The computed temperatures $T(x_m, y_m, t)$ at the sensor locations are compared to the measurements' histories $Y_m(t)$. Accurate results are obtained, providing that the experimental data are carefully determined. In practice, all these data are available for the experimental conditions described above, except the values of the heat transfer coefficient $h(T)$ which are roughly approximated from empirical laws [18,19].

As it will be illustrated in the following sections, the solutions of the IHSP computed with the additional data $Y_m(t)$ are very sensitive to errors in the coefficient $h(T)$. That is why an inverse boundary coefficient problem (IBCP) is analyzed first. It consists in estimating the function $h(T)$ on Γ_1 from the same additional data $Y_m(t)$. Moreover, by using the same method to solve both the problems IHSP and IBCP, we illustrate how the CGA combined to finite element technique is a very powerful and general approach to estimate unknown functions for solving two-dimensional IHCPs.

3. Inverse problems

3.1. The conjugate gradient algorithm

Let $\underline{h} = [h_i]_{i=1}^{Np}$, $\underline{F} = [x_1, y_1, x_2, y_2]$ and $\underline{P} = \left[P_1^1, P_1^2, \ldots, P_1^{Nt}, P_2^1, P_2^2, \ldots, P_2^{Nt}\right]$ be, respectively, the vectors of parameters introduced in the notation of the following functions:

- $h(T) = \sum_{i=1}^{Np} h_i\varphi_i(T)$,
- $F_i(x,y) = 1/\pi\omega^2 \exp\left[-\frac{(x-x_i)^2+(y-y_i)^2}{\omega^2}\right], \quad i=1,2,$
- $P_i(t_k) = P_i^k, \quad k=1,\ldots,Nt, \ i=1,2.$

The inverse analysis of the heat conduction problem aims to determine the unknown part denoted by $\underline{U}$ of the vectors $(\underline{h}, \underline{F}, \underline{P})$ from the additional data $Y_m(t_k), k=1,\ldots,Nt; m=1,\ldots,Ns$, given by the temperature sensors during the experiments. The inverse problems are formulated in the least-square sense and consists in finding the optimal solution which minimizes the functional

$$J(\underline{U}) = \frac{1}{2}\int_0^{t_f}\sum_{m=1}^{Ns}\left(T(x_m,y_m,t;\underline{U}) - Y_m(t)\right)^2 \mathrm{d}t, \tag{6}$$

where $T(x_m, y_m, t; \underline{U})$ is the solution of Eqs. (2a)–(2d). The solutions of two separated inverse problems have been searched for

- the IBCP: $\underline{U} = (\underline{h})$, $\underline{F}$ and $\underline{P}$ are fixed to its experimental values,
- the IHSP: $\underline{U} = (\underline{F}, \underline{P})$, $\underline{h}$ is fixed to the estimated values, solution of the above IBCP.

Other combinations could be investigated, for example $\underline{U} = (\underline{h}, \underline{P})$ and $\underline{F}$ are fixed to their experimental values, etc. However, the CGA is described for the general case, then applications to particular cases are deduced.

The CGA is iterative. At each iteration n, the previous estimate $\underline{U}^n$ is corrected according to

$$\underline{U}^{n+1} = \underline{U}^n - \gamma_n\underline{d}^n \text{ in order to have } J\left(\underline{U}^{n+1}\right) < J(\underline{U}^n), \tag{7}$$

where $\underline{d}^n$ is the search direction, and γ^n is a positive scalar. Let $\underline{J}'$ be the vector gradient of the functional $J(\underline{U})$. Depending on the definition of $\underline{U}$, the components of $\underline{J}'$ are taken from the following set:

$$J'_{hj} = \frac{\partial J}{\partial h_j}, \quad j=1,2,\ldots,Np, \tag{8a}$$

$$J'_{x_i} = \frac{\partial J}{\partial x_i}, \quad i=1,2, \tag{8b}$$

$$J'_{y_i} = \frac{\partial J}{\partial y_i}, \quad i=1,2, \tag{8c}$$

$$J'_{P_i^k} = \frac{\partial J}{\partial P_i^k}, \quad i=1,2; \ k=1,\ldots,Nt. \tag{8d}$$

The vector $\underline{d}^n$ and the scalar γ_n are determined according to the conjugate gradient equations

$$\underline{d}^n = \underline{J}'^n + \beta^n\underline{J}'^{n-1}, \tag{9a}$$

$$\beta^0 = 0, \tag{9b}$$

$$\beta^n = \frac{\langle \underline{J}^n, \underline{J}^n - \underline{J}^{n-1} \rangle}{\|\underline{J}^n\|}, \tag{9c}$$

where $\|\cdot\|$ is the norm associated to the scalar product $\langle .,. \rangle$

$$\gamma^n = \frac{\sum_{m=1}^{Ns} \int_0^{t_f} \delta T^n(x_m, y_m, t; \underline{U})(T^n(x_m, y_m, t; \underline{U}) - Y_m(t))\,\mathrm{d}t}{\sum_{m=1}^{Ns} (\delta T^n(x_m, y_m, t; \underline{U}))^2}, \tag{10}$$

where δT^n is the sensitivity function at the iteration n, resulting from the variations $\underline{\delta U}$. The sensitivity function $\delta T^n(x_m, y_m, t; \underline{U})$ evaluated at the sensor locations, and the gradient vector $\underline{J}'$ are determined by solving, respectively, the sensitivity equations and the adjoint equations.

3.2. Sensitivity equations

Let $\varepsilon\underline{\delta U}$ be a variation of $\underline{U}$, the resulting varied temperature is denoted by $T_\varepsilon^+ = T(\underline{U} + \varepsilon\underline{\delta U})$. The sensitivity function is defined by

$$\delta T = \lim_{\varepsilon \to 0} \frac{T_\varepsilon^+ - T}{\varepsilon}. \tag{11}$$

Writing Eqs. (2a)–(2d) for the solution T_ε^+, subtracting these same equations for the solution T, the limiting process $(\varepsilon \to 0)$ leads to the following sensitivity equations:

$$\frac{\partial(\rho C_p \delta T)}{\partial t} - \lambda \Delta \delta T = \delta S, \quad t > 0 \text{ in } \Omega, \tag{12a}$$

$$\lambda \frac{\partial \delta T}{\partial n_1} + \left(h(T) + \frac{\partial h}{\partial T}(T - T_e) \right) \delta T = \left(\sum_{i=1}^{Np} \delta h_i \varphi_i(T) \right)(T_e - T), \quad t > 0 \text{ in } \Gamma_1, \tag{12b}$$

$$\lambda \frac{\partial \delta T}{\partial n_2} = 0, \quad t > 0 \text{ in } \Gamma_2, \tag{12c}$$

$$\delta T = 0, \quad t = 0 \text{ in } \Omega, \tag{12d}$$

where

$$\delta S = \sum_{i=1}^{2} \left(F_i \delta P_i + P_i \left(\frac{\partial F_i}{\partial x_i} \delta x_i + \frac{\partial F_i}{\partial y_i} \delta y_i \right) \right). \tag{13}$$

In Eqs. (12a)–(12d) and (13), the general case has been considered, all the components of $\underline{h}$, $\underline{F}$ and $\underline{P}$ are varying simultaneously. In practice, only the components of the unknown vector $\underline{U}$ are varied. For example, if $\underline{U} = \underline{h}$, (IBCP), then $\delta\underline{F}$ and $\delta\underline{P}$ are taken equal to zero.

The resulting variation δJ of the functional J is

$$\delta J(\underline{U}) = \sum_{m=1}^{Ns} \int_0^{t_f} \int_\Omega (T(x_m, y_m, t; \underline{U}) - Y_m(t)) \delta(x - x_m) \delta(y - y_m) \delta T \,\mathrm{d}t \,\mathrm{d}\Omega. \tag{14}$$

Furthermore, by definition, the components of the gradient vector are satisfied by

$$\delta J(\underline{U}) = \sum_{j=1}^{Np} J'_{h_j} \delta h_j + \sum_{i=1}^{2} \left(J'_{x_i} \delta x_i + J'_{y_i} \delta y_i + \int_{t=0}^{t_f} J'_{P_i}(t) \delta P_i \,\mathrm{d}t \right), \tag{15}$$

then, in order to compute the components $J'_{h_j}, J'_{x_i}, J'_{y_i}, J'_{P_i}$, Eq. (14) has to be put in the form of Eq. (15). This is usually done by introducing a Lagrangian.

3.3. Lagrangian and adjoint equations

Let $L(T, \underline{h}, \underline{F}, \underline{P})$ be the Lagrangian associated to the optimization problem defined by Eq. (6) and the constraint (2a)

$$L(T, \underline{h}, \underline{F}, \underline{P}, \psi) = J(T) + \int_0^{t_f} \int_\Omega \psi \left[\rho C_p \frac{\partial T}{\partial t} - \lambda \Delta T - S \right] \mathrm{d}t \,\mathrm{d}\Omega, \tag{16}$$

where $\psi(x, y, t)$ is a Lagrange multiplier. More general definition of L may be introduced to take into account the other constraints (2b)–(2d), but for simplicity of presentation, the function T is supposed to satisfy these constraints.

When ψ is fixed, the differential of L is

$$\delta L = \int_0^{t_f} \int_\Omega E \delta T \,\mathrm{d}t \,\mathrm{d}\Omega + \int_0^{t_f} \int_\Omega \left(\frac{\partial(\rho C \delta T)}{\partial t} - \lambda \Delta \delta T - \delta S \right) \psi \,\mathrm{d}t \,\mathrm{d}\Omega, \tag{17}$$

where

$$E(x, y, t; \underline{U}) = \sum_{m=1}^{Ns} (T(x, y, t; \underline{h}, \underline{F}, \underline{P}) - Y_m(t)) \delta(x - x_m) \delta(y - y_m). \tag{18}$$

Integration by parts gives

$$\int_0^{t_f} \int_\Omega \frac{\partial(\rho C \delta T)}{\partial t} \psi \,\mathrm{d}t \,\mathrm{d}\Omega = \int_\Omega [\rho C \psi \delta T]_{t=0}^{t=t_f} \,\mathrm{d}\Omega - \int_0^{t_f} \int_\Omega \rho C \frac{\partial \psi}{\partial t} \,\mathrm{d}t \,\mathrm{d}\Omega \tag{19}$$

and

$$\int_0^{t_f} \int_\Omega \lambda \psi \Delta \delta T \,\mathrm{d}t \,\mathrm{d}\Omega = \int_0^{t_f} \int_\Gamma \lambda \frac{\partial \delta T}{\partial n} \psi \,\mathrm{d}\Gamma - \int_0^{t_f} \int_\Gamma \lambda \frac{\partial \psi}{\partial n} \delta T \,\mathrm{d}\Gamma + \int_0^{t_f} \int_\Omega \lambda \delta T \Delta \psi \,\mathrm{d}t \,\mathrm{d}\Omega. \tag{20}$$

If T satisfies the constraints' equations (2b)–(2d), then δT satisfies the Eqs. (12b)–(12d) and by using the Eqs. (19) and (20), the differential δL, Eq. (17), takes the new form

$$\begin{aligned}\delta L = & \int_0^{t_f}\int_\Omega \left(-\rho C\frac{\partial\psi}{\partial t}-\lambda\Delta\psi+E\right)\delta T\,\mathrm{d}t\,\mathrm{d}\Omega \\ & + \int_\Omega [\rho C\psi\delta T]_{t_f}\,\mathrm{d}\Omega \\ & + \int_0^{t_f}\int_{\Gamma_1}\left(\lambda\frac{\partial\psi}{\partial n_1}+\left(h+\frac{\mathrm{d}h}{\mathrm{d}T}(T-T_e)\right)\psi\right)\delta T\,\mathrm{d}t\,\mathrm{d}\Gamma_1 \\ & + \int_0^{t_f}\int_{\Gamma_2}\lambda\frac{\partial\psi}{\partial n_2}\delta T\,\mathrm{d}t\,\mathrm{d}\Gamma_2 - \int_0^{t_f}\int_\Omega \delta S\psi\,\mathrm{d}t\,\mathrm{d}\Omega \\ & - \int_0^{t_f}\int_{\Gamma_1}(T-T_e)\psi\left(\sum_{i=1}^{Np}\delta h_i\varphi_i(T)\right)\mathrm{d}t\,\mathrm{d}\Gamma_1. \qquad (21)\end{aligned}$$

The Lagrange multiplier ψ is fixed in order to satisfy the following equation (the so-called adjoint equation):

$$\frac{\partial L}{\partial T}\delta T = 0 \quad \forall\delta T, \qquad (22)$$

where this condition consists in fixing to zero the first four terms of Eq. (21) and leads to take ψ solution of the following equations:

$$-\rho C_p\frac{\partial\psi}{\partial t}-\lambda\Delta\psi = E, \quad t>0,\ (x,y)\in\Omega, \qquad (23a)$$

$$\lambda\frac{\partial\psi}{\partial n_1}+\left(h(T)+\frac{\partial h}{\partial T}(T-T_e)\right)\psi = 0, \quad t>0,\ (x,y)\in\Gamma_1, \qquad (23b)$$

$$\frac{\partial\psi}{\partial n_2} = 0, \quad t>0,\ (x,y)\in\Gamma_2, \qquad (23c)$$

$$\psi = 0, \quad t=t_f,\ (x,y)\in\Omega. \qquad (23d)$$

The "source" function E in Eq. (23a) is equal to zero almost everywhere in Ω except at the sensor locations (x_m,y_m), where it is equal to the deviation between the computed temperature and the measurements (Eq. (18)).

3.4. Components of the gradient

Taking T solution of Eqs. (2a)–(2d), and ψ solution of Eqs. (23a)–(23d), it becomes

$$\begin{aligned}\delta J = \delta L = & -\int_0^{t_f}\int_\Omega \psi\delta S\,\mathrm{d}t\,\mathrm{d}\Omega \\ & -\int_0^{t_f}\int_{\Gamma_1}(T-T_e)\psi\left(\sum_{i=1}^{Np}\delta h_i\varphi_i(T)\right)\mathrm{d}t\,\mathrm{d}\Gamma_1,\end{aligned} \qquad (24)$$

then, δJ can be put in the desired form of Eq. (15)

$$\delta J = \sum_{j=1}^{Np}\frac{\partial L}{\partial h_j}\delta h_j + \sum_{i=1}^{2}\left(\frac{\partial L}{\partial x_i}\delta x_i+\frac{\partial L}{\partial y_i}\delta y_i+\sum_{k=0}^{Nt}\frac{\partial L}{\partial P_i^k}\delta P_i^k\right). \qquad (25)$$

The computation of the terms $\partial L/\partial h_j, \partial L/\partial x_i, \partial L/\partial y_i$, $\partial L/\partial P_i^k$ are derived from Eqs. (24) and (13)

$$J'_{h_j} = -\int_0^{t_f}\int_{\Gamma_1}\psi(T-T_e)\varphi_j(T)\,\mathrm{d}t\,\mathrm{d}\Gamma_1, \quad j=1,2\ldots,Np, \qquad (26a)$$

$$J'_{x_i} = -\int_0^{t_f}\int_\Omega \psi P_i\frac{\partial F_i}{\partial x_i}\,\mathrm{d}t\,\mathrm{d}\Omega, \quad i=1,2, \qquad (26b)$$

$$J'_{y_i} = -\int_0^{t_f}\int_\Omega \psi P_i\frac{\partial F_i}{\partial y_i}\,\mathrm{d}t\,\mathrm{d}\Omega, \quad i=1,2, \qquad (26c)$$

$$J'_{P_i^k} = -\int_\Omega \psi P_i^k\,\mathrm{d}\Omega, \quad i=1,2, \qquad (26d)$$

$$\frac{\partial F_i}{\partial x_i} = -\frac{2(x-x_i)}{\omega^2}F_i. \qquad (27)$$

More details can be found in [20], especially for the non-linear cases including temperature-varying parameters $\rho C_p(T)$ and $\lambda(T)$ in Eqs. (2a)–(2d).

3.5. Algorithm

It is available for solving both the IBCP and the IHSP:

- For the IBCP, ($\underline{U}=\underline{h}$), $\underline{F}$ and $\underline{P}$ are fixed, then the components of the gradient J'_{x_i}, J'_{y_i} and J'_{P_i}, $i=1,2$ are taken as equal to zero, and only Eq. (26a) is computed.
- For the IHSP, $\underline{U}=(\underline{F},\underline{P})$ and $\underline{h}$ is fixed, then the components J'_{h_j}, $j=1,\ldots,Np$ are taken as equal to zero, and only Eqs. (26b)–(26d) are computed.

The iterative structure of the algorithm is as follows:

(a) $n\leftarrow 0$; Choose an initial guess $\underline{U}^0$.

(b) Repeat:

- solve the direct problem, Eqs. (2a)–(2d), to compute $T(x_m,y_m,t,\underline{U})$ and the functional $J=J(\underline{U})$, Eq. (6),
- solve the adjoint Eqs. (23a)–(23d), to compute the components of the gradient, Eqs. (26a)–(26d),
- solve the sensitivity Eqs. (12a)–(12d), to compute the new iterate, Eqs. (7) and (10),
- $n\leftarrow n+1$; until $J^n\leqslant\varepsilon$

(c) end

ε is a positive scalar which is chosen depending on the variance of the temperature measurement errors to avoid unstable solutions, according to the iterative regularizing principle [2].

4. Solution of the IHSP – numerical experiments

In this section, the influence of the heat transfer coefficient on the solution of the IHSP is shown. Only the heat source S_1 is supposed to be unknown. A finite element solver is used to compute the solutions of the direct, the adjoint and the sensitivity equations. A regular grid of the domain Ω is considered from $21 \times 21 = 441$ nodes. The time interval is $[0, 2000\ \text{s}]$, the time step is $\Delta t = 25$ s The heat transfer coefficient depends on the temperature, $\underline{h}$ is fixed to the values of the piecewise linear function shown in Fig. 3 (case #1).

The temperature values T_0 and T_e are taken as equal to 20°C. The strength $P_2(t)$ is held at zero, the strength $P_1(t)$ and the resulting temperature histories $Y_m(t); m = 1, \ldots, 4$ used to solve the IHSP are shown in Fig. 4(a). In Fig. 4(b), it is shown how the temperature $T(x, y, t)$ at $t_k = 1500$ s is spatially varying. It must be observed that on the boundary Γ_1, close to the point heat source S_1, variations of temperature are important and lead to significant variations of the heat transfer coefficient. The maximum temperature rise is $T_{\max} = 80$°C, therefore, $h(T)$ must be known from the temperature range $[T_0, T_{\max}]$, which is greater than the temperature interval scanned by the thermocouples.

The point source S_2 is assumed to be known. To examine the influence of systematic errors, four solutions of the IHSP are computed and compared:

- case #1: the solution is computed with the exact values of $\underline{h}$;
- cases #2 and #3: the solution is computed with the biased values of $\underline{h}$;
- case #4: the solution is computed with the average of the exact values of $\underline{h}$.

For each case studied, Figs. 5 and 6 show, respectively, the location (x_1^n, y_1^n) computed at each iteration n of the minimization process, and the final estimated strength $P_1(t)$.

The initial guess is $x_1^0 = 12$ mm, $y_1^0 = 11$ mm, $P_1^0(t_k) = 0\ \forall k$.

The main results of these numerical experiments are:

- without systematic errors on $\underline{h}$ (case #1), it is possible to estimate simultaneously the location and the strength of the source, the estimated source location is equal to the exact location ($x_1^{\text{exact}} = 18.86$ mm, $y_1^{\text{exact}} = 19.84$ mm), see Fig. 5(a); and the estimated strength is very close to the exact values (Fig. 6),
- with biased values of $\underline{h}$, cases #2 and #3, the estimated location is also equal to the exact location, Figs. 5(b) and (c), but the estimated strength is biased (Fig. 6),
- with a constant heat transfer coefficient equal to the exact average value of $\underline{h}$, case #4, both the estimated location and strength are biased, the computed solution is ($x_1 = 18.39$ mm, $y_1 = 19.21$ mm) (Fig. 5(d)).

It is observed that bias on the heat transfer coefficient $h(T)$ and on the estimated strength $P_1(t)$ are highly correlated. During heating, by taking $h(T)$ as greater

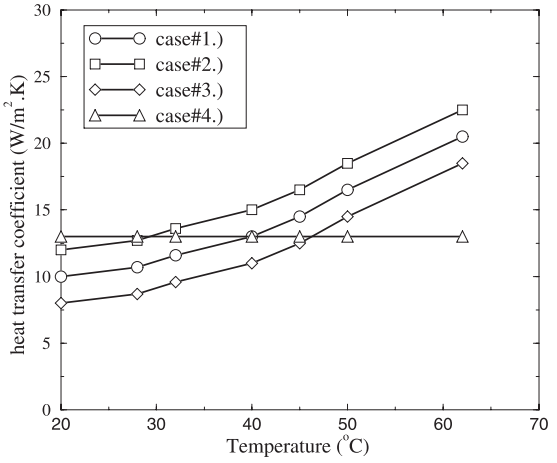

Fig. 3. Numerical experiment – heat transfer coefficient.

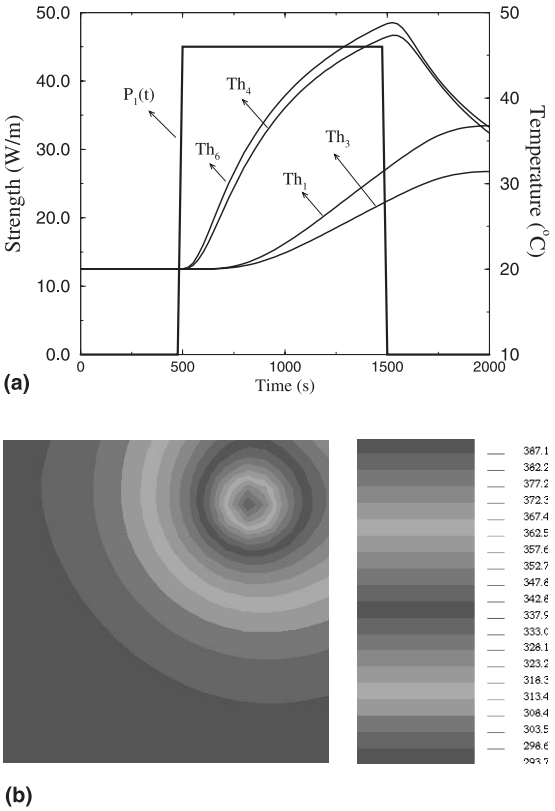

Fig. 4. Numerical experiment: (a) time-varying strength $P_1(t)$ of the heat source S_1 and temperature histories computed at the locations of thermocouples $\text{Th}_1, \text{Th}_3, \text{Th}_4, \text{Th}_6$; (b) temperature field $T(xy, t)$ (in K) at $t = 1500$ s.

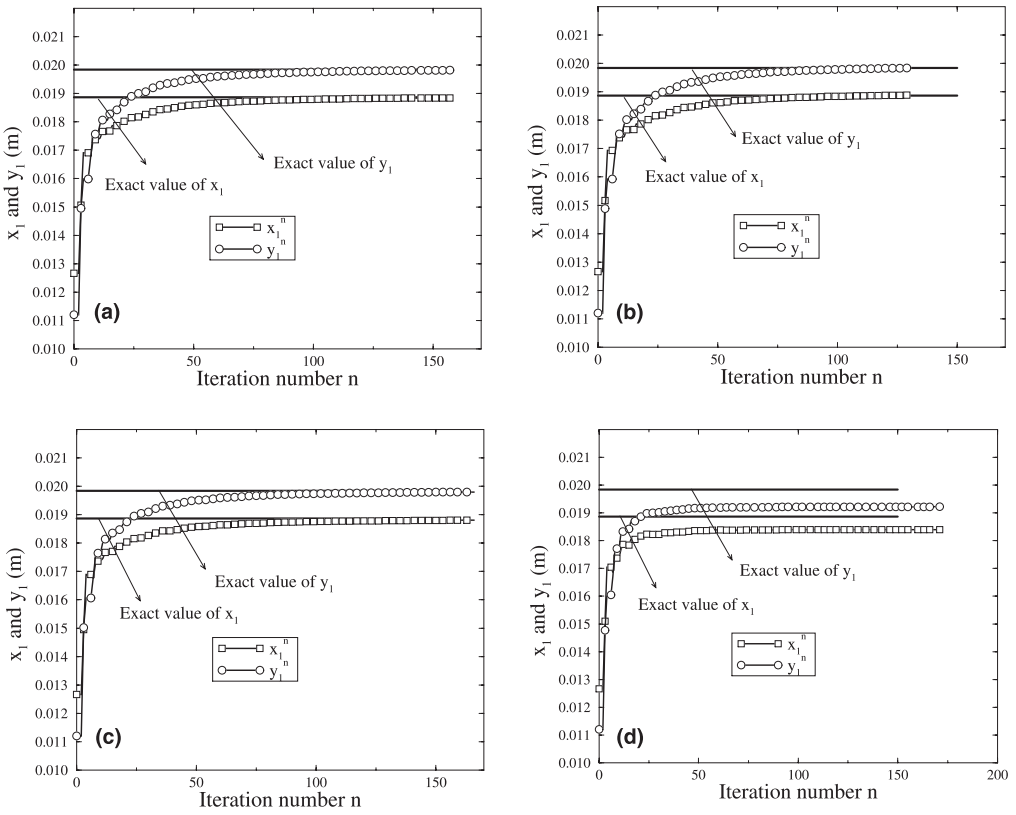

Fig. 5. Numerical experiment – estimated location (x_1, y_1) at each iteration n: (a) case #1, exact value of $\underline{h}$; (b) case #2, biased value of $\underline{h}$; (c) case #3, biased value of $\underline{h}$; (d) case #4, average value of $\underline{h}$.

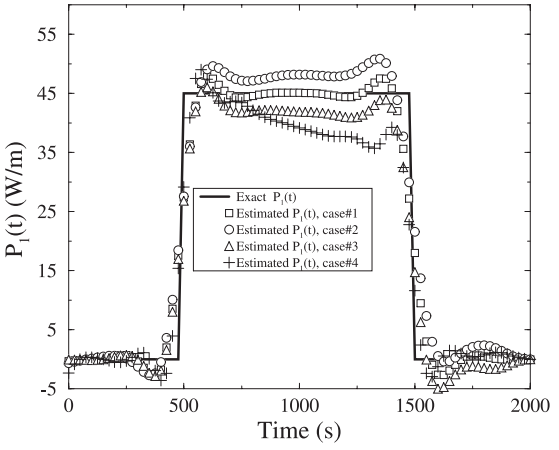

Fig. 6. Numerical experiment – estimated strength $P_1(t)$.

than $h_{\text{exact}}(T)$ (case #2), the heat losses computed at the boundary with the exact strength are greater than the true losses, then the inverse algorithm compensates the bias on $h(T)$ by increasing the estimated strength in order to balance the computed heat losses and to match the temperatures at the sensor locations. The same reasoning is valid for $h(T)$ less than $h_{\text{exact}}(T)$, in that case, the inverse algorithm underestimates the strength $P_1(t)$. Moreover, when the variations of h with temperature are neglected, then the estimated location of the point source is biased and the strength is underestimated.

These results illustrate that for the experimental conditions considered, the variation of the heat transfer coefficient with the temperature cannot be neglected and it must be accurately known to estimate simultaneously the location and the strength of the source. That is why the experimental study begins with the resolution of the IBCP, to estimate correct values of $\underline{h}$.

5. Experimental results: solutions of the IBCP and the IHSP

5.1. Solution of the IBCP

The determination of the temperature-varying heat transfer coefficient $\underline{h}$ from the measured temperature $Y_m(t)$ was achieved under the conditions summarized in Fig. 7,

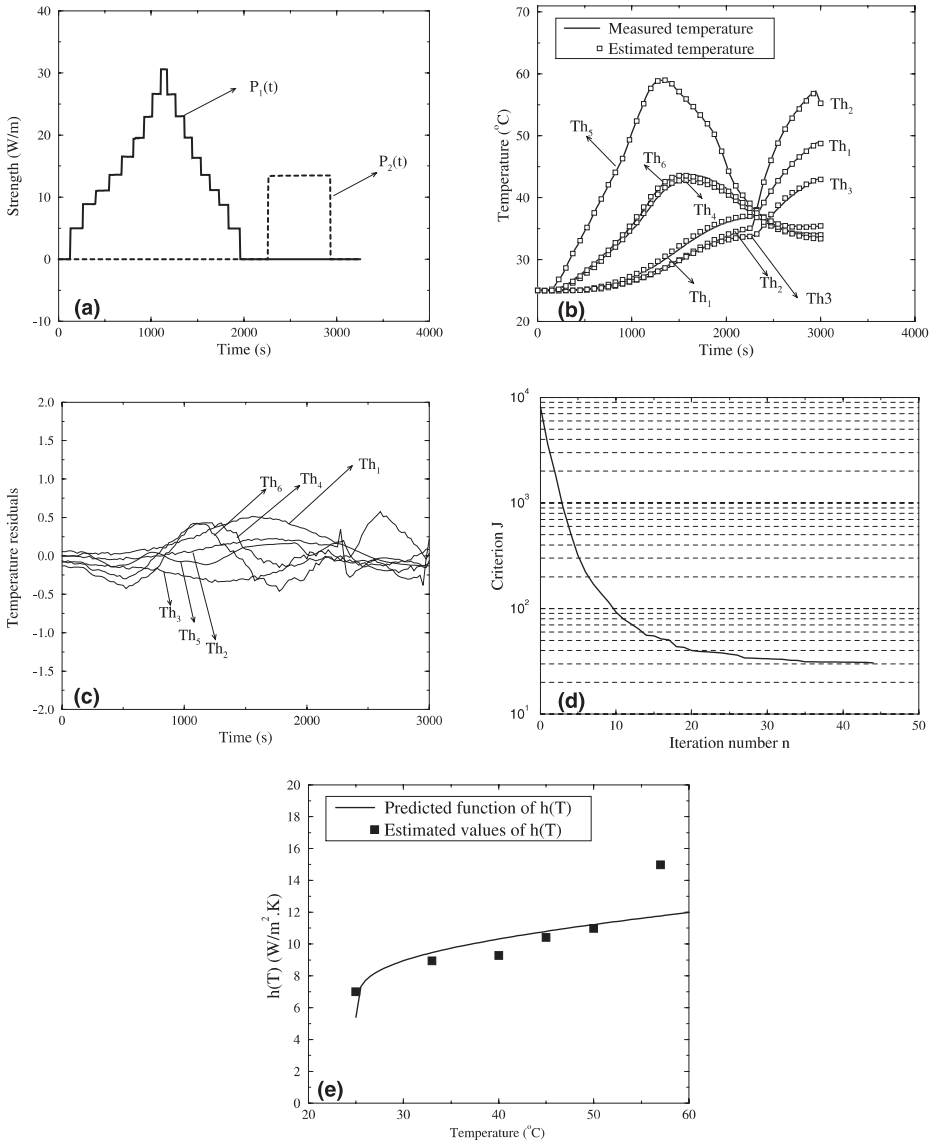

Fig. 7. Experimental results – solution of the IBCP: (a) strength $P_1(t)$ and $P_2(t)$ during heating; (b) measured and estimated temperatures at $n = 17$; (c) temperature residuals vs time; (d) criterion J vs iteration number n; (e) estimated and predicted values of $h(T)$.

the duration of the experiment is $t_f = 3000$ s, the time steps is $\Delta t = 25$ s and the number of time steps is $Nt = 120$, the time-varying strengths $P_1(t)$ and $P_2(t)$ and the resulting temperature evolutions of thermocouples $Th_1, Th_2, Th_3, Th_4, Th_5, Th_6$ are shown in Figs. 7(a) and (b).

The maximum temperature rise is observed by the sensor Th_5, it is less than 60°C. A piecewise linear function with $Np = 6$, is chosen to estimate $h(T)$ the temperature range of the experiment (25°C, 58°C). The initial guess is taken to the constant value $h(T) = 6$ W/m^2 K. Figs. 7(c) and (d) illustrate the iterative resolution of the IBCP, the criterion $J(\underline{h}^n)$ is decreasing and reaches a plateau. The application of the iterative regularization principle consists in stopping iterations at the optimal number n_{opt} which satisfies

$$J_{\text{opt}} = J(\underline{h}^n)_{n=n_{\text{opt}}} = NtNs\sigma^2, \tag{28}$$

where σ is an estimation of the standard deviation of the temperature residuals. For this experiment, the temperature residuals, Fig. 7(c), have a zero mean value, and σ is estimated to 0.25°C

$$J_{\text{opt}} = 120 \times 6 \times (0.25)^2 = 45.$$

From the curve shown in Fig. 7(d), this value of J_{opt} corresponds to $n_{\text{opt}} = 17$. The final estimation of $h_n(T)$ at $n = n_{\text{opt}}$ is an increasing function shown in Fig. 7(e).

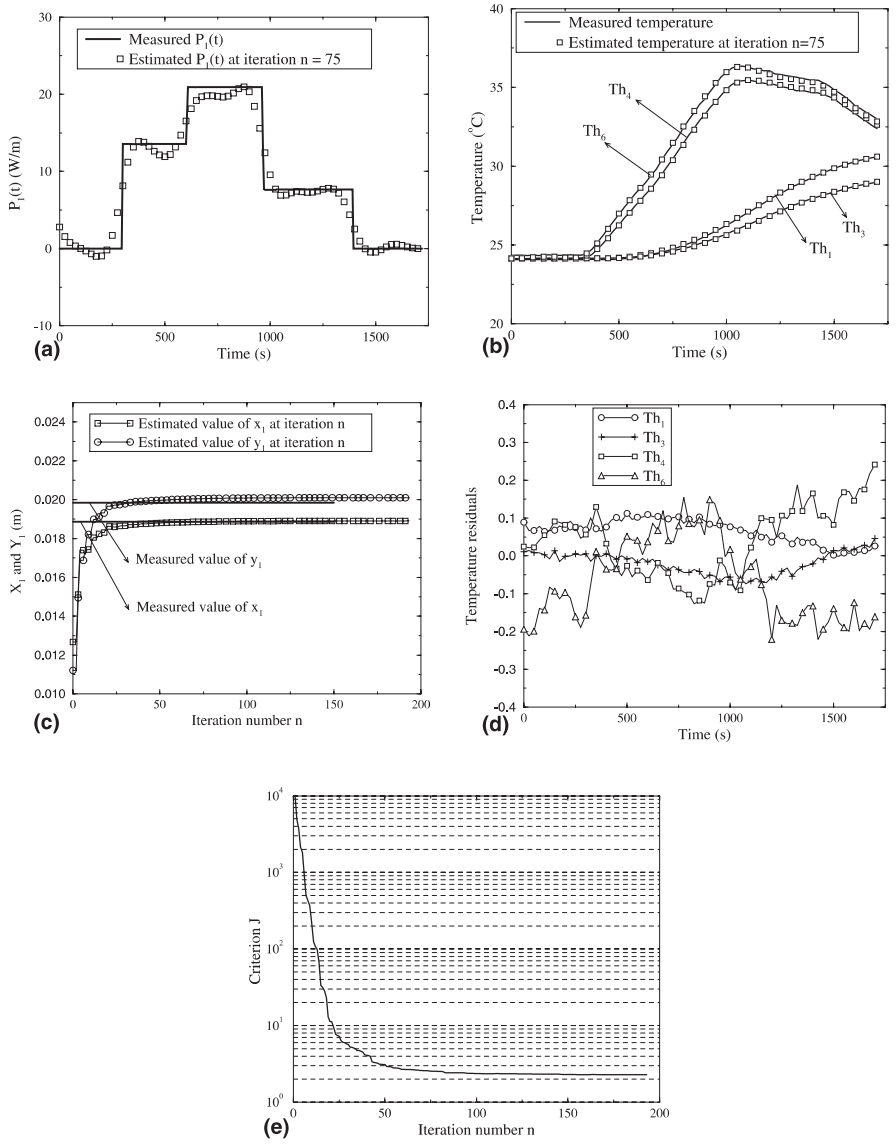

Fig. 8. Experimental results – solution of the IHSP (experiment #1): (a) measured and estimated strength $P_1(t)$; (b) measured and calculated temperatures at $n = 75$; (c) estimated location of S_1 at each iteration n; (d) temperature residuals vs time; (e) criterion J vs iteration number n.

This estimated function is compared to the predicted values obtained by the following laws [18,19]:

$$h(T) = 1.42\left(\frac{T - T_e}{H}\right)^{0.25} + \varepsilon_r 5.67 \times 10^{-8}(T^2 + T_e^2)(T + T_e) \times (\varepsilon_r = 0.95,\ T_e = 25°\mathrm{C}). \quad (29)$$

In Fig. 7(e), the deviation between the estimated and the predicted values of $h(T)$ is lesser than 6%, except for temperatures greater than 55°C. This experiment has been repeated with different time-varying strengths $P_1(t)$ and the computed solutions of the IBCP take the same form as in Fig. 7(e). These experimental results show that heat flux on the boundary Γ_1 is accurately modeled by a Fourier condition and that the correct estimate of the function $h(T)$ can be computed by solving the IBCP. This estimated function will be used now to solve different cases of the inverse heat source problems.

5.2. Solutions of the IHSP

The results of three experiments are presented. The simultaneous determination of the location and the

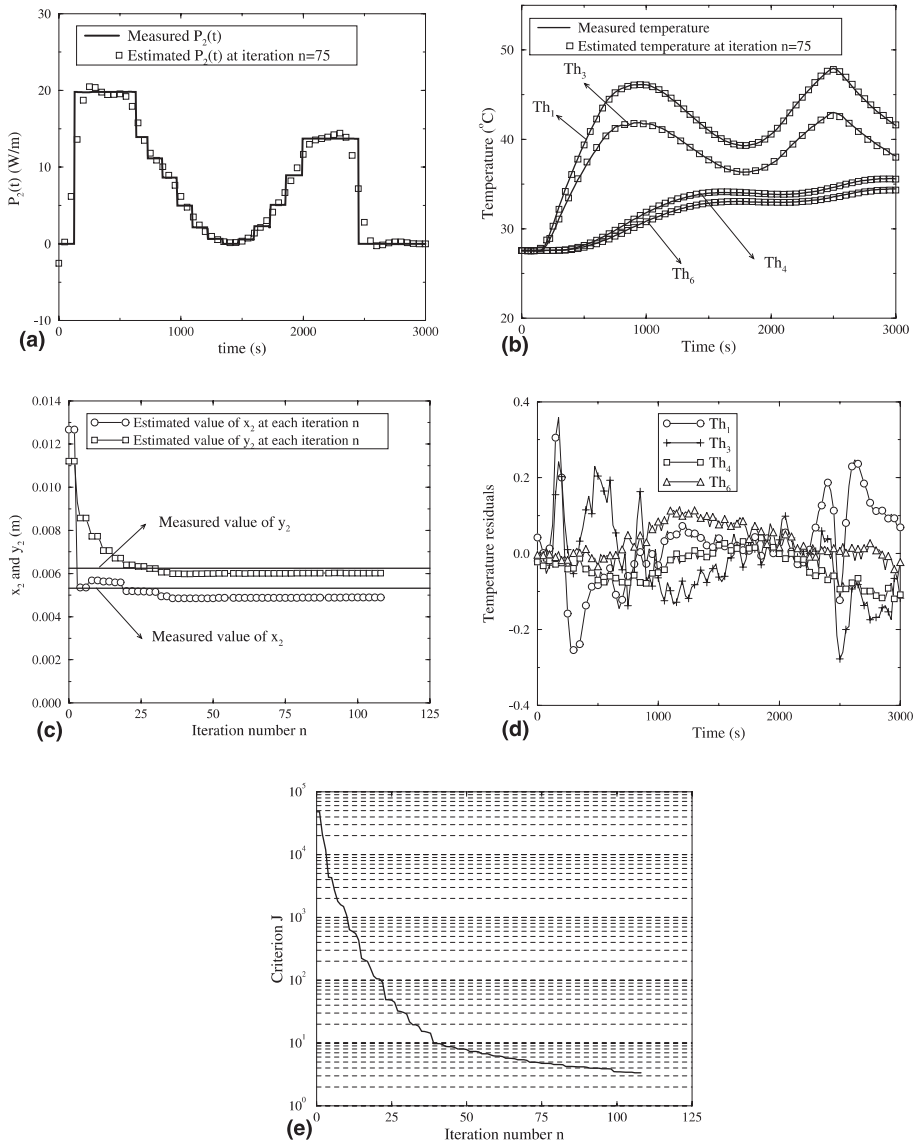

Fig. 9. Experimental results – solution of the IHSP (experiment #2): (a) measured and estimated $P_2(t)$; (b) measured and calculated temperatures at $n = 75$; (c) estimated location of S_2 at each iteration n; (d) temperature residuals vs time; (e) criterion J vs iteration number n.

strength of only one heat source is studied first. Each point source S_1 or S_2 is considered separately (experiment #1 and #2). Then, the determination of the location of the bi-source is investigated (experiment #3).

Experiment #1. The location (x_1, y_1) and the strength $P_1(t), 0 < t < t_f$ are determined simultaneously. Results are summarized in Fig. 8. The duration of the experiment is $t_f = 1700$ s, the number of time steps is $Nt = 68$. The IHSP is solved by taking the measurements $Y_m(t)$, Fig. 8(b), from thermocouples $\mathrm{Th}_1, \mathrm{Th}_3, \mathrm{Th}_4$, and Th_6. In Fig. 8(d), we find that standard deviation of the temperature residuals is $\sigma = 0.1°\mathrm{C}$. According to the above practical rule of the iterative regularization principle, the optimal value of the criterion is

$$J_{\mathrm{opt}} = 68 \times 4 \times (0.1)^2 = 2.72,$$

then, from Fig. 8(e), the optimal number of iterations is $n_{\mathrm{opt}} = 75$.

The solution of IHSP estimated location (x_1, y_1) and estimated strength $P_1(t)$ at iteration $n_{\mathrm{opt}} = 75$ are shown in Figs. 8(a) and (c). The deviations between the estimated location and the experimental values are

$$\Delta x_1 = | x_1^{n_{opt}} - x_1^{exact} | = 10^{-5} \text{ m};$$

$$\Delta y_1 = | y_1^{n_{opt}} - y_1^{exact} | = 16 \times 10^{-5} \text{ m}.$$

Both the location and the strength estimations of the source S_1 are very correct, Δx_1 and Δy_1 are less than the wire radius of the line source.

Experiment #2. The locations (x_2, y_2) and the strength $P_2(t), 0 < t < t_f$ are determined simultaneously. Results are summarized in Fig. 9. The duration of the experiment is 3000 s, the number of time steps is $Nt = 120$. The IHSP is solved by taking the measurements $Y_m(t)$ (Fig. 9(b)), from thermocouples Th_1, Th_3, Th_4, and Th_6. In Fig. 9(d), we find that the standard deviation of the temperature residuals is also $\sigma = 0.1°C$. In the same way as above, it is found that $J_{opt} = 4.8$ and Fig. 9(e) leads to an optimal number of iterations $n_{opt} = 75$.

The solution of IHSP estimated location (x_2, y_2) and estimated strength $P_2(t)$ at iteration $n_{opt} = 75$, are shown in Figs. 9(a) and (c). The deviations between the estimated location and the experimental values are

$$\Delta x_2 = | x_2^{n_{opt}} - x_2^{exact} | = 45 \times 10^{-5} \text{ m};$$

$$\Delta y_2 = | y_2^{n_{opt}} - y_2^{exact} | = 24 \times 10^{-5} \text{ m}.$$

Both the location and strength estimations of the source S_2 are correct. Δx_2 is equal to the wire diameter, the accuracy is worse than in experiment #1.

Fig. 10(a) shows the estimated temperature field at $t = 1000$ s for experiment #1 and Fig. 10(b) shows the estimated temperature field at $t = 2500$ s for experiment #2, we can observe that the temperature T in the domain Ω is less than $T_{max} = 120°C$, so, the law used for $C_P(T)$ is valid (Eq. (29)). We can also observe the strong variation of temperature on the boundary of the domain Ω close to the point source S_2.

Experiment #3. Both the locations (x_1, y_2) and (x_2, y_2) are determined simultaneously. The measured strengths $P_1(t)$ and $P_2(t)$ shown in Fig. 11(a) are considered to be known. The duration of the experiment is 2500 s, the number of time steps is $Nt = 90$. The temperature measurements are shown in Fig. 11(b). We have carried out two resolutions of this IHSP, first by using the temperature measurements of the six thermocouples, and the second by using the temperature measurements of four thermocouples Th_1, Th_3, Th_4, Th_6.

Fig. 11(c) shows the solution of IHCP obtained with each iteration by using the temperature measurements of six thermocouples. The deviations between the estimated locations and the experimental values at $n = 11$ are smaller than the radius of the wire

$$\Delta x_1 = 16 \times 10^{-5} \text{ m}; \quad \Delta y_1 = 24 \times 10^{-5} \text{ m};$$

$$\Delta x_2 = 25 \times 10^{-5} \text{ m}; \quad \Delta y_2 = 19 \times 10^{-5} \text{ m}.$$

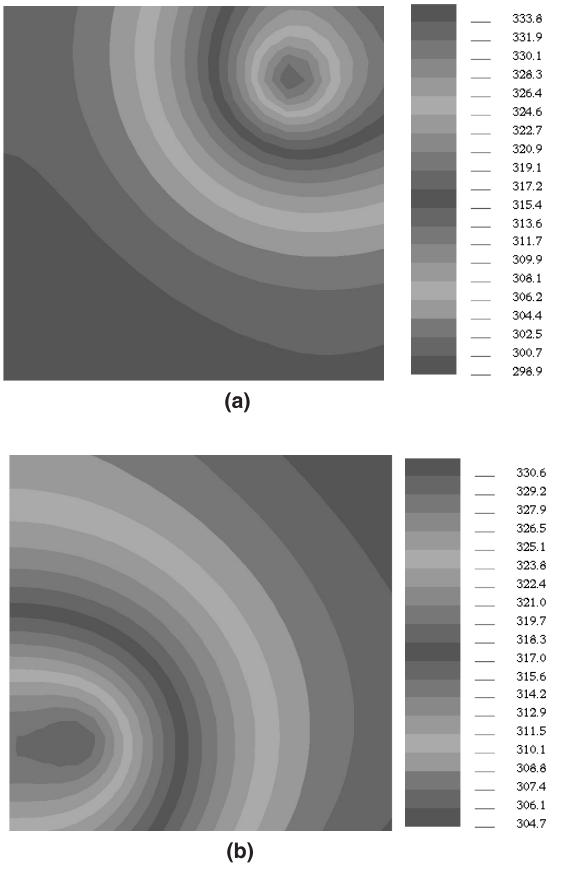

Fig. 10. Estimated temperature field $T(x, y, t)$ (in K): (a) for experiment #1 at $t = 1000$ s; (b) for experiment #2 at $t = 2500$ s.

These experimental results are very correct. It is possible to determine simultanously the locations of S_1 and S_2 by using the six temperature measurements of the six thermocouples.

Fig. 11(d) shows the solution of IHCP obtained with each iteration by using the temperature measurements of four thermocouples. The deviations between the estimated locations and the experimental values at $n = 23$ are

$$\Delta x_1 = 66 \times 10^{-5} \text{ m}; \quad \Delta y_1 = 80 \times 10^{-5} \text{ m};$$

$$\Delta x_2 = 8 \times 10^{-5} \text{ m}; \quad \Delta y_2 = 17 \times 10^{-5} \text{ m}.$$

The computed solution of IHSP by using four thermocouples is less precise than that obtained by using six thermocouples. The inverse problem which consists in determining simultaneously the location and the strength of two-point sources is more difficult. From a computational point of view, no unique solution can be determined for this experiment.

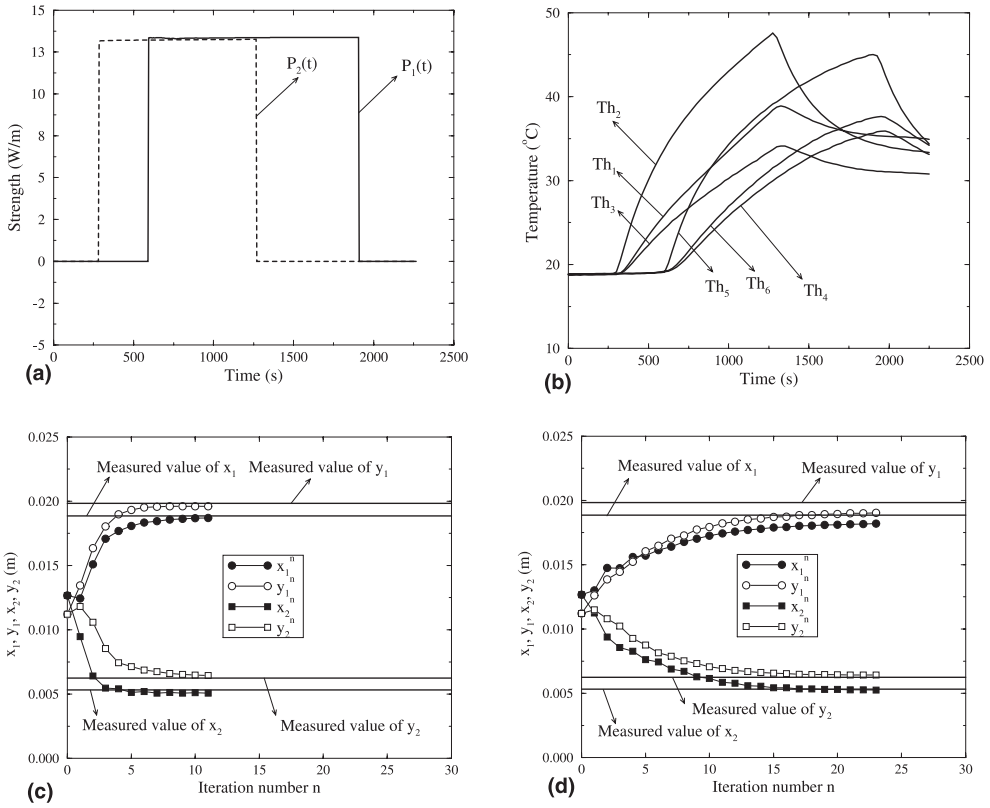

Fig. 11. Experimental results – solution of the IHSP (experiment #3): (a) strength $P_1(t)$ and $P_2(t)$ during heating; (b) measured temperature; (c) estimated location of S_1 and S_2 at each iteration n by using the six thermocouples; (d) estimated location of S_1 and S_2 at each iteration n by using four thermocouples Th_1, Th_3, Th_4, Th_6.

6. Conclusion

The well-known CGA has been used for solving two-dimensional IHCPs. Combined with finite element technique, the results show that this numerical method is powerful, and well adapted to perform inverse heat flow analysis in various situations, especially for arbitrarily shaped bodies and non-linear problems with temperature-varying properties. The method has been applied for the determination of a heat transfer coefficient depending on temperature, as well as for the determination of functions of the independent variables (space and time) like the location and the strength of point heat sources. In comparison of past research on IHSPs, the presented results illustrate that the method is also valid to estimate simultaneously the location and the strength of the sources. An important question concerning the uniqueness of the solution remains open. It was observed for example that the estimation problem of the location and the strength of a bi-source has no unique solution under the considered experimental conditions. Experimental results have shown that heat flux on the boundary is accurately modeled by a Fourier condition and that a good estimation of the function $h(T)$ is required to avoid biased solutions to the IHSP.

References

[1] J.V. Beck, Inverse Heat Conduction. Ill-posed Problems, Wiley/Interscience, New York, 1985.
[2] O.M. Alifanov, Inverse Heat Transfer Problems, Springer, Berlin, 1994.
[3] Y. Jarny, M.N. Ozisik, J.P. Bardon, A general optimization method using adjoint equation for solving multidimensional inverse heat conduction, Int. J. Heat Mass Transfer 34 (1991) 2911–2919.
[4] A. Osman, J. Beck, Investigation of transient heat transfer coefficient in quenching experiments, J. Heat Transfer 112 (1990) 843–848.
[5] S. Das, A.J. Paul, Determination of interfacial heat transfer coefficient in casting and quenching using a solution technique for inverse problems based on the boundary element method, Metall. Trans. B (Process Metallurgy) 24 (1993) 1077–1086.
[6] N. Zabaras, G.Z. Yang, Inverse design of solidification desired with freezing front motion and heat fluxes, in: Proceedings of the Second International Conference on

Inverse Problem in Engineering, Le Croisic, France, pp. 545–555.
[7] C.H. Huang, T.M. Ju, A.A. Tseng, The estimation of surface thermal behavior of working roll in hot rolling process, Int. J. Heat Mass Transfer 38 (1995) 1019–1031.
[8] N. Al-Khalidy, J. Skorek, An extended Kalaman filter-control volume method for solving inverse heat conduction problems in a moving body, Bulletin of the Polish Academy of Sciences (Technical Sciences) 44 (1995) 39–53.
[9] S. Peneau, J.P. Humeau, Y. Jarny, Front motion and convective heat flux determination in a phase change process, Inverse Problem Eng. 4 (1996) 53–91.
[10] A.J. Silva Neto, M.N. Ozisik, Two-dimensional inverse heat conduction problem of estimating the time-varying strength of a line heat source, J. Appl. Phys. 71 (1992) 5357–5362.
[11] C. Le Niliot, The boundary-element method for the time-varying strength estimation of point heat sources: application to a two-dimensional diffusion system, Numer. Heat Transfer B 33 (1998) 301–321.
[12] C. Le Niliot, P. Gallet, Infrared thermography applied to the resolution of inverse heat conduction problems: recovery of heat line sources and boundary conditions, Rev. Gen. Therm. 37 (1998) 629–643.
[13] C.-Y. Yang, The determination of two heat sources in an inverse heat conduction problem, Int. J. Heat Mass Transfer 42 (1999) 345–356.
[14] M. Ohmichi, N. Noda, Inverse analysis of two-dimensional steady-state heat conduction problem with many plane heat sources, Trans. Information Processing Soc. Jpn., 36 (1995) 2566–2572.
[15] R. Abou Khachfe, Y. Jarny, Résolution numérique d'un problème d'estimation de source thermodépendante dans un domaine bidimensionnel, congrés SFT, Arcachon, France, Elsevier, 1999, pp. 3–7.
[16] R. Abou Khachfe, Y. Jarny, Estimation of heat sources within two dimensional shaped bodies, in: Proceedings of the Third International Conference on Inverse Problems Engineering, June 1999, Port Ludlow, Washington, DC, USA.
[17] T. Jurkowski, Y. Jarny, D. Delauny, Estimation of thermal conductivity of thermoplastics under moulding conditions: an apparatus and an inverse algorithm, Int. J. Heat Mass Transfer 40 (1997) 4169–4181.
[18] Y. Bayazitoglu, M.N. Ozisik, Elements of Heat Transfer, McGraw-Hill, New York, 1988.
[19] Y. Bayazitoglu, M.N. Ozisik, Int. J. Heat Mass Transfer 40 (1997) 4169–4181.
[20] R. Abou khachfe, Y. Jarny, Numerical solution of 2-D non-linear inverse heat conduction problems using finite element techniques, Numer. Heat Transfer B 37 (2000) 45–68.